

## Improvement of Corrosion Resistance and Magnetic Properties of NdFeB Sintered Magnets with Cu and Zr Co-Added

Minxiang Pan, Pengyue Zhang\*, Qiong Wu, Hongliang Ge

Magnetism key laboratory of Zhejiang Province, China Jiliang University, Hangzhou 310018, China

\*E-mail: [zhang\\_pengyue@cjl.u.edu.cn](mailto:zhang_pengyue@cjl.u.edu.cn)

Received: 26 January 2016 / Accepted: 22 February 2016 / Published: 1 March 2016

---

Cu and Zr powders are co-added as intergranular modifiers to improve the corrosion resistance of the NdFeB sintered magnets. Compared with the Cu and Zr free sample, the  $E_{\text{corr}}$  is increased sharply from -0.799 V to -0.697 V for the co-added sample with 0.15 wt.% Cu and 0.85 wt.% Zr, which demonstrate that small additions of Cu and Zr co-added can remarkably improve the electrochemical stability and corrosion resistance in salt solution. Besides, Co and Zr co-addition proved to result in relevant improvement in the magnetic properties, especially in the coercivity  $H_{\text{cj}}$ ,  $H_{\text{cj}}$  was improved from 2000 to 2181 kA/m at room temperature. Further investigation of temperature dependence of coercivity demonstrates that Cu and Zr co-addition sample shows a larger  $|\beta|$  compared to that of the Cu and Zr free sample.

---

**Keywords:** Corrosion, Magnetic properties, Sintered magnet

### 1. INTRODUCTION

Since the development of the NdFeB sintered magnets, it attracts much attention due to the high anisotropy and magnetic properties. As compared to the SmCo magnets, the NdFeB sintered magnets have higher magnetic properties, such as coercivity  $H_{\text{cj}}=5572$  kA/m [1-6]. A high coercivity is always expected for the sintered NdFeB magnets in terms of the high magnetic crystallization anisotropy, but the experimental value of the coercivity is only about 2000 kA/m-3000 kA/m is considerably smaller than the theoretical predictions  $H_{\text{cj}} = 7164$  kA/m [2,3]. Therefore, many works have been carried out to solve the problem that refining the microstructure and optimizing the manufacturing method.

In addition, it is well known that the NdFeB magnets applications are also limited by the poor corrosion resistance, which is due to the electrochemical potential of Nd-rich phase is much lower than that of hard magnetic  $\text{Nd}_2\text{Fe}_{14}\text{B}$  phase [7,8]. Many efforts have been working towards solving these

problem by the surface coating or the elements addition [9,10]. Unfortunately, most of efforts lead to the reduction of remanence for the corrosion resistance enhanced. So, it is necessary to find some other elements to improve the corrosion resistance of magnets without remanence reduction.

In this work, we reported the effects of Cu and Zr powders are co-added as intergranular modifiers on the corrosion resistance, microstructure and magnetic properties of the NdFeB sintered magnets by HD method. Meanwhile, the effect of Cu and Zr co-addition on the temperature dependence of coercivity are systematically analyzed.

## 2. EXPERIMENTAL PART

Alloys with nominal composition of  $(\text{Nd,Pr})_{14.65}\text{Fe}_{79.11}\text{Nb}_{0.21}\text{B}_{6.03}$  (wt.%) were prepared by vacuum induction melting of highly pure Nd, Fe metals (purity 99.9%), Pr-Nd (Pr 20 at.%),  $\text{Fe}_3\text{B}$  (B 19.3 at.%), and NbFe (Nb 66.3 at.%) under the protection of highly-purity argon atmosphere. The ingots were then subjected in rectangular water-cooled copper molds. The alloys were crushed by a standard hydrogen decrepitated (HD) treatment, followed by jet milling to produce fine powders with an average particle size of  $\sim 4.8\mu\text{m}$ . The powders were then blended with micro-sized Cu and Zr powders for 2 h under nitrogen atmosphere. After blending, the mixed powders were compacted at 6 MPa in a magnetic field of 1.6 T. The green compacts were sintered for 3 h at  $1180^\circ\text{C}$ , followed by a two-step annealing treatment, which was performed for 3 h at  $930^\circ\text{C}$  and for 5 h at  $550^\circ\text{C}$ , respectively.

The microstructure of these magnets was examined by X-ray diffraction (XRD) with a Cu  $K\alpha$  radiation. The magnetic properties of the final samples with the size  $\Phi 10*10$  mm were measured by the Pulsed Field Magnetometer (PFM). Polarization curves were determined with a PARSTAT 2273 advance electrochemical system. Each measurement was performed using two electrode cell consisting of NdFeB sintered magnets working electrode and Pt counter electrode. All experiments were conducted at  $23^\circ\text{C}$  in 2.5 wt.% NaCl aqueous solution. The potential scan rate was 2 mV/s along the direction from the negative potential to the positive one. Accelerated corrosion test was performed by placing cubic samples ( $10\text{mm}*10\text{mm}*10\text{mm}$ ) in  $120^\circ\text{C}$ , 2 bar and 100% relative humid atmosphere for 24, 48, 72 and 96 h, respectively. The mass losses of the corrosion test were measured weighing the sample before and after the corrosion test with removing the corrosion products from the sample surfaces by using the microbalance.

To study the intensity of crystal texture, the pole density factor  $P_{(hkl)}^H$  was calculated according to the Horta method [5]:

$$P_{(hkl)}^H = \frac{\left[ \sum_1^n M_{(hkl)} \right] \cdot I_{(hkl)} / I_{R(hkl)}}{\sum_1^n \left[ M_{(hkl)} \cdot I_{(hkl)} / I_{R(hkl)} \right]} \quad (1)$$

where  $I_{(hkl)}$  is the measured intensity of the  $(hkl)$  crystal face,  $M_{(hkl)}$  is the multiplicity of the  $(hkl)$  crystal face,  $I_{R(hkl)}$  represents the equational intensity of the  $(hkl)$  crystal face.

## 3. RESULTS AND DISCUSSION

Fig.1 shows the potentiodynamic polarization curves for the NdFeB sintered magnets measured in 2.5 wt.% NaCl aqueous solutions. It can be found that all of the samples exhibit typical hydrogen

evolution polarization in the cathodic region and the anodic sides are controlled by the active dissolution [11]. Their corresponding corrosion potential  $E_{\text{corr}}$ , corrosion current density  $i_{\text{corr}}$  and Tafel slope were obtained by the Tafel extrapolation method [12], which were illustrated in Table 1. Compared with the Cu and Zr free sample, the  $E_{\text{corr}}$  is increased sharply from -0.799 V to -0.697 V for the co-added sample with 0.15 wt.% Cu and 0.85 wt.% Zr. Meanwhile, it can be seen clearly that the Cu and Zr co-added sample has a lower corrosion current density,  $i_{\text{corr}} = 16.86 \mu\text{A}/\text{cm}^2$ , and Tafel slope,  $b = 115 \text{ mV}/\text{dec}$ , compared with the Cu and Zr free sample ( $i_{\text{corr}} = 32.58 \mu\text{A}/\text{cm}^2$  and  $b = 143 \text{ mV}/\text{dec}$ ). These demonstrate that small additions of Cu and Zr co-added can remarkably improve the electrochemical stability and corrosion resistance in salt solution. Additionally, as 1.0 wt.% Zr is added, the  $E_{\text{corr}}$  also becomes more positive, the corrosion current density  $i_{\text{corr}}$  and Tafel slope get lower, compared with the Cu and Zr free sample. Hence the magnet added with Zr also possesses better corrosion resistance than the starting magnet.

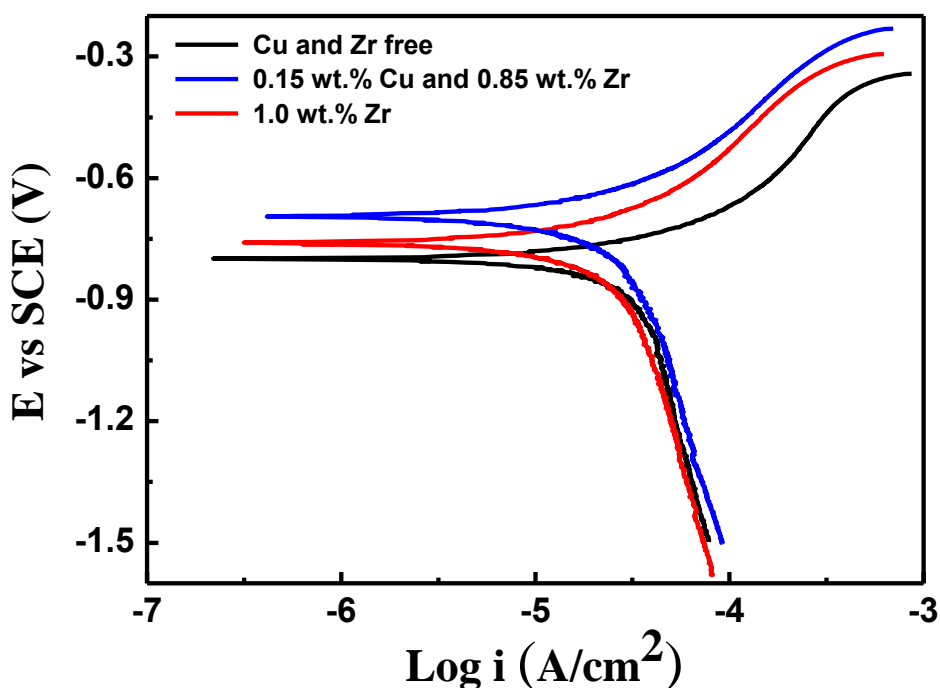


**Figure 1.** Potentiodynamic polarization curves in 2.5 wt.% NaCl aqueous solutions for the different NdFeB sintered magnets.

**Table 1.** The corrosion potential  $E_{\text{corr}}$ , corrosion current density  $i_{\text{corr}}$  and Tafel slope  $b$  of NdFeB sintered magnets tested in 2.5 wt.% NaCl aqueous solutions.

Additive	$E_{\text{corr}}(\text{V})$	$i_{\text{corr}}(\mu\text{A}/\text{cm}^2)$	$b(\text{mV}/\text{dec})$
Cu and Zr free	-0.799	32.58	143
0.15 wt.% Cu and 0.85 wt.% Zr	-0.697	16.86	115
1.0 wt.% Zr	-0.755	19.01	127

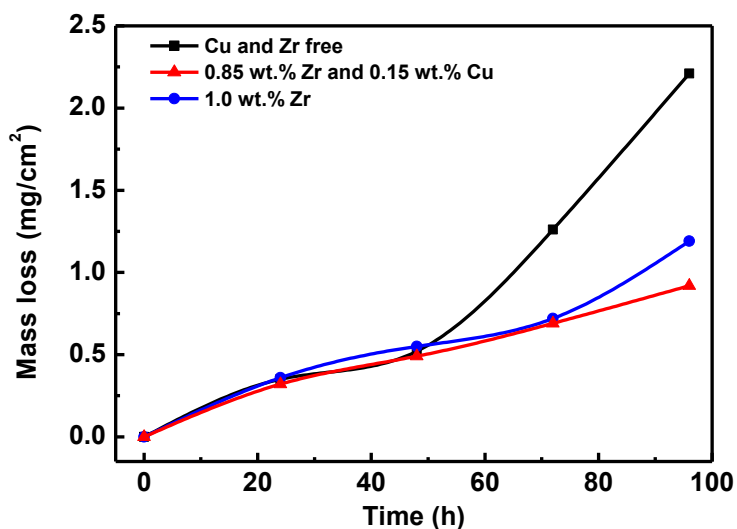


**Figure 2.** Mass loss of the NdFeB sintered magnets measured in 120°C, 2 bar and 100% relative humidity atmosphere for different times.

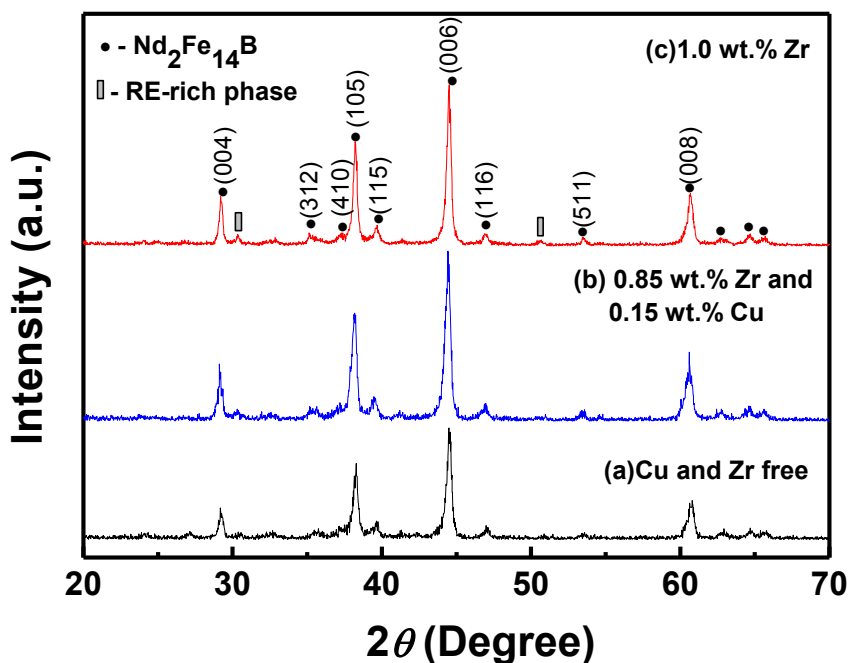


**Figure 3.** XRD patterns of the starting magnet (a), the magnet with 0.85 wt.% Zr and 0.15 wt.% Cu co-addition (b) and the magnet with 1.0 wt.% Zr addition (c) in the perpendicular direction of the magnetic field.

The improvement of the corrosion resistance for the NdFeB sintered magnets is also reflected by the mass loss tests in hot and humid atmosphere. Fig. 2 displays the mass loss as a function of the exposure time for different magnets in 120°C, 2 bar and 100% relative humidity atmosphere. As can be seen, all of the samples have a nearly negligible mass loss of  $\sim 0.5 \text{ mg/cm}^2$  before 48 h. When the exposure time was further prolonged to 96 h, the mass loss of Cu and Zr free sample reaches to  $\sim 2.3$

mg/cm<sup>2</sup>. However, for the sample with 1.0 wt.% Zr addition, the mass loss decreases to ~1.2 mg/cm<sup>2</sup> at 96 h. When Cu is co-added with Zr, the mass loss reduces drastically to ~0.9 mg/cm<sup>2</sup>, which is only about 1/2 of the Cu and Zr free sample. Results show that small co-addition of Cu and Zr can remarkably improve the corrosion resistance of the NdFeB sintered magnets in hot/humid atmosphere, which may be attributed to the intergranular RE-rich phase change by the small addition, similar to the reported results for NdFeB sintered magnets by intergranular addition [13,14].

In addition to the improved corrosion resistance, the microstructure are also well retained by Cu and Zr co-added, as shown by the XRD patterns in Fig. 3. A detailed analysis of the XRD patterns shows that all of the magnets are composed of hard magnetic phase Nd<sub>2</sub>Fe<sub>14</sub>B (*P42/mnm*) and a trace of the Nd-rich phase. Moreover, the intensities of the (004), (006), (008) crystal faces of the Nd<sub>2</sub>Fe<sub>14</sub>B crystals were much stronger as compared with that of the (410) crystal face (See Fig. 3 (a), (b) and (c)). It demonstrates that a strong (001) texture is formed in the NdFeB sintered magnets. Similar results were also observed in the sintered magnets with other intergranular addition [15,16]. To illustrate the intensity of the (001) texture of the Nd<sub>2</sub>Fe<sub>14</sub>B crystals in the NdFeB sintered magnets, the pole density factors of (001) crystal faces were calculated in term of Horta-formula (Eq. 1). The results showed that the pole density factors of (004), (006), (008) crystal faces for the starting NdFeB magnets were 3.12, 4.17, 5.37, respectively, which were higher than for the 0.85 wt.% Zr and 0.15 wt.% Cu co-addition sample (2.63, 3.66 and 3.98) and 1.0 wt.% Zr addition sample (2.17, 3.25 and 3.85). This result indicates that the intensity of the orientation is decreased with the co-addition of Cu and Zr.

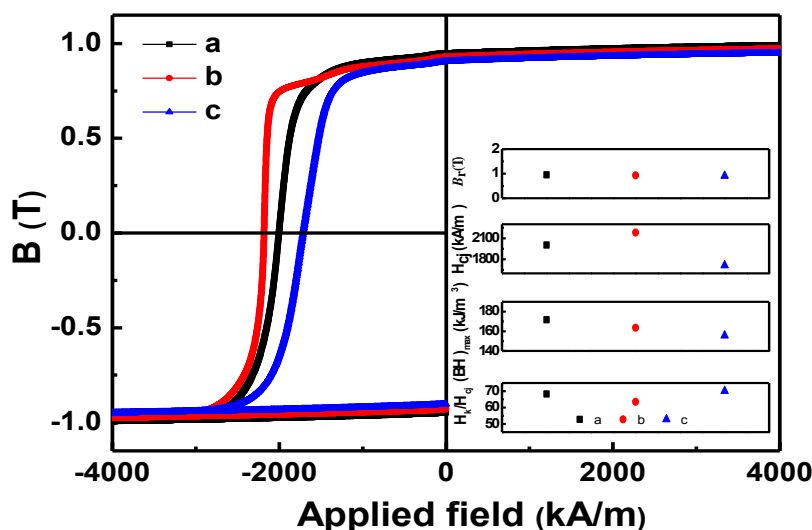


**Figure 4.** Demagnetization curves of the starting magnet (a), the magnet with 0.85 wt.% Zr and 0.15 wt.% Cu co-addition (b) and the magnet with 1.0 wt.% Zr addition (c). Insets: the magnetic properties as a function of different addition.

Fig. 4 shows the demagnetization curves of the starting magnet and Cu/Zr co-addition. It can be seen that the starting magnet and 1.0 wt.% Zr addition magnet show a typical single-phase behavior, indicating a good intergrain exchange-coupling in these magnet. A similar trend with NdCu adding is observed in the NdFeB sintered magnet by Chen *et. al.* [17]. However, for the sample with Cu and Zr

are co-added a kink appears in the demagnetization curve, this suggests that the magnetization reversal of the hard magnetic phase occurs independently. This result leads to a deterioration of squareness for the hysteresis loops. Meanwhile, the insets of Fig. 4 summarizes the magnetic properties as a function of different addition. Compared to the starting NdFeB sintered magnet, the Cu and Zr co-added sample shows a strong increase in coercivity  $H_{cj}$  from 2000 to 2181 kA/m. For the 1.0 wt.% Zr addition sample, although the highest squareness ( $H_k/H_{cj}$ : 70.1) was achieved, the other three physical quantities ( $B_r$ ,  $(BH)_{max}$ ,  $H_{cj}$ ) show a slowly decrease. In conclusion, although the NdFeB sintered magnet with Cu and Zr co-added tends to result in an strong increase in coercivity  $H_{cj}$  and almost constant of remanence  $B_r$ , the highest maximum energy product  $(BH)_{max}$  was not achieved as a reason of “a kink” in the demagnetization curve.

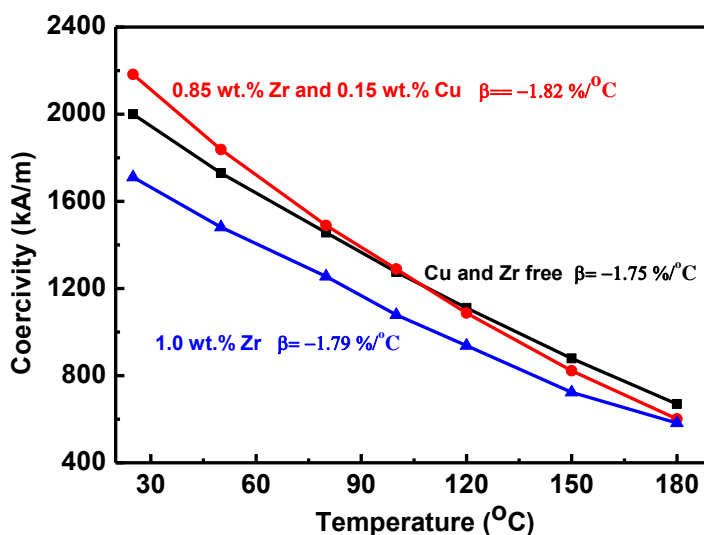


**Figure 5.** Temperature dependence of coercivity for the NdFeB sintered magnets.

Fig. 5 shows the temperature dependence of coercivity  $H_{cj}$  for the NdFeB sintered magnets. It can be seen that the coercivity decreases much quicker with increasing temperature for the magnets with Cu and Zr co-added. Meanwhile, the temperature coefficient of coercivity,  $\beta = [\Delta H_c / H_c \Delta T] \times 100$ , calculated from 25°C to 180°C for the starting magnet, the Cu and Zr co-addition magnet, and 1.0 wt.% Zr addition magnet were -1.75%/°C, -1.82%/°C, and -1.79%/°C, respectively. Although the room temperature of the coercivity is improved by the Cu and Zr co-addition, the sample shows a larger  $|\beta|$  compared to that of the Cu and Zr free sample.

#### 4. CONCLUSION

Corrosion resistance of NdFeB sintered magnets can be improved by co-addition of Cu and Zr powders via the intergranular addition technology. The mass loss of Cu and Zr co-addition sample in hot and humid environments for 96 h is only 1/2 of the Cu and Zr free magnet. Compared with the Cu

and Zr free sample, the  $E_{\text{corr}}$  is also increased sharply from -0.799 V to -0.697 V for the co-added sample with 0.15 wt.% Cu and 0.85 wt.% Zr, which demonstrate that small additions of Cu and Zr co-added can remarkably improve the electrochemical stability and corrosion resistance in salt solution. Besides, Co and Zr co-addition proved to result in relevant improvement in the magnetic properties, especially in the coercivity  $H_{\text{cj}}$ .

#### ACKNOWLEDGEMENT

This work was supported by the Provincial Natural Science Foundation (Nos. LQ15E010005 and LR15E010001), and the National Science Foundation of China (Nos.51371163 and 51301158).

#### Reference

1. I. Wnuk, J. J. Wysocki, *J. Mater. Processing Tech*, 175 (2006) 433
2. T. H. Kim, S. R. Lee, M. W. Lee, T. S. Jang, J. W. Kim, Y. D. Kim, H. J. Kim, *Acta Mater*, 66 (2014) 12
3. H. Sepehri-Amin, T. Ohkubo, T. Shima, K. Hono, *Acta Mater*, 60 (2012) 819
4. N. J. Harrison, H. A. Davies, I. Todd, *J. Appl. Phys*, 99 (2006) 08B504
5. P. L. Wu, X. H. Li, W. Li, H. Y. Sun, Y. Chen, X. Y. Zhang, *Mater. Lett*, 62 (2008) 309
6. X. Fang, Y. Shi, D. C. Jiles, *IEEE trans. Magn*, 34 (1998) 1291
7. H. R. Madaah Hosseini, A. Dadoo, A. Dolati, A. Kianvash, *J. Alloys Compd*, 419 (2006) 337
8. Y. Matsuura, J. Hoshijima, R. Ishii, *J. Magn. Magn. Mater*, 336 (2013) 88
9. A. A. El-Moneim, A. Gebert, M. Uhlemann, O. Gutfleisch, L. Schultz, *Corros. Sci*, 44 (2002) 1857
10. C. Sun, W. Q. Liu, H. Sun, M. Yue, X. F. Yi, J. W. Chen, *J. Mater. Sci. Technol*, 28 (2012) 927
11. A. Gebert, A.A. El-Moneim, O. Gutfleisch, L. Schultz, *IEEE Trans. Magn*, 38 (2002) 2979
12. X. G. Cui, M. Yan, T. Y. Ma, L. Q. Yu, *Physica B*, 403 (2008) 4182
13. P. Zhang, L. P. Liang, J. Y. Jin, Y. J. Zhang, X. L. Liu, M. Yan, *J. Alloys Compd*, 616 (2014) 345
14. Y. R. Wu, J. J. Ni, T. Y. Ma, M. Yan, *Physica B*, 405 (2010) 3303
15. C. X. Jin, R. J. Chen, W. Z. Yin, X. Tang, Z. X. Wang, J. Y. Ju, D. Lee, A. R. Yan, *J. Magn. Magn. Mater*, 670 (2016) 72
16. Z. H. Hu, H. Dong, D. W. Ma, C. Luo, *J. Magn. Magn. Mater*, 401 (2016) 169
17. F. G. Chen, T. Q. Zhang, J. Wang, L. T. Zhang, G. F. Zhou, *Scripta. Mater*, 107 (2015) 38

© 2016 The Authors. Published by ESG ([www.electrochemsci.org](http://www.electrochemsci.org)). This article is an open access article distributed under the terms and conditions of the Creative Commons Attribution license (<http://creativecommons.org/licenses/by/4.0/>).